European Journal of Radiology 199 (2026) 112795

Contents lists available at ScienceDirect

European Journal of Radiology

journal homepage: www.elsevier.com/locate/ejrad

NeuroMix-DL: Improving imaging quality of a fast multiparametric MRI protocol using deep learning

Amirhossein Sanaat [a,b,*], Johannes Hugo Decker [b], Ramy Hussein [b], Moss Y Zhao [b], Habib Zaidi [a,c,d,e], Tim Sprenger [f,g], Stefan Skare [g], Michael Moseley [b], Greg Zaharchuk [b]

[a] Division of Nuclear Medicine and Molecular Imaging, Geneva University Hospital, Geneva, Switzerland
[b] Department of Radiology, Stanford University, Stanford, CA 94305, USA
[c] Department of Nuclear Medicine and Molecular Imaging, University of Groningen, University Medical Center Groningen, Groningen, Netherlands
[d] Department of Nuclear Medicine, University of Southern Denmark, Odense, Denmark
[e] University Research and Innovation Center, Óbuda University, Budapest, Hungary
[f] MR Applied Science Laboratory Europe, GE Healthcare, Stockholm, Sweden
[g] Department of Neuroradiology, Karolinska University Hospital, Stockholm, Sweden

ARTICLE INFO

Keywords:
MRI
Brain imaging
Image quality
NeuroMix
Transformers

ABSTRACT

Purpose: To improve the quality of a fast multi-contrast MR protocol acquisition using deep learning.
Materials and methods: 350 patients (age: 64 ± 17 yrs; 155 male) underwent both a fast brain MR multi-contrast sequence (NeuroMix), capturing five contrasts in a single 2.5-minute sequence, and conventional high-resolution imaging. This retrospective study was approved by the Stanford IRB (eProtocol 26147, IRB registration 6208). The paired images were used to enhance resolution and image quality using a Swin U-Net Transformer (SwinUNETR) approach, focusing on T1-weighted (T1w), T2-weighted (T2w), and T2 FLAIR images (NeuroMix-DL). Evaluation included standard image quality metrics, such as the root mean squared error (RMSE) and a clinical quality assessment using a five-point image quality scale (1 = poor, 5 = excellent). A pairwise *t*-test was calculated to evaluate the values of the qualitative and quantitative metrics across the various image processing approaches.
Results: We found significant improvement in image quality after applying the trained SwinUNETR, with RMSE reductions of 42 ± 3%, 33 ± 2%, and 33 ± 9% for T1w, T2w, and FLAIR images, respectively ($p < 0.001$ for all) compared to original NeuroMix images, using conventional sequences as reference. The clinical readers found higher image quality scores for NeuroMix-DL images compared to the original NeuroMix images (12 ± 8%, 17 ± 11%, and 15 ± 6% for T1w, T2w, and FLAIR images, respectively). Visual quality assessment demonstrated improvements in prevalent artifacts, including motion, herringbone artifact, inhomogeneity artifact, and RF overflow.
Conclusion: The SwinUNETR model offers a viable approach for improving the quality of fast multi-contrast MR images while effectively mitigating artifacts, improving the cost-benefit ratio of MRI.

1. Introduction

Magnetic resonance imaging (MRI) plays an important role in non-invasive neuroimaging because of its excellent qualitative and quantitative performance. However, its longer acquisition time can cause patient discomfort and motion, impacting satisfaction and anxiety levels during scans for up to 30% of patients, mainly due to claustrophobia [1]. Faster scans can significantly enhance patient tolerance and satisfaction during MRI procedures.

Several strategies have been explored to truncate the MRI scanning time. These methods can be divided into conventional/analytical methods and AI methods. The conventional methods include echo planar imaging (EPI) [2], EPIMix [3], compressed sensing [4], parallel imaging [5], radial k-space sampling [6], self-navigated techniques [7], and stack-of-stars acquisition [8]. These methods can lead to geometric distortion and signal dropouts due to magnetic field inhomogeneities

* Corresponding author at: Division of Nuclear Medicine and Molecular Imaging, Geneva University Hospital, Rue Gabrielle-Perret-Gentil 4, 1205 Geneva, Switzerland.
E-mail address: Amirhossein.sanaat@unige.ch (A. Sanaat).

https://doi.org/10.1016/j.ejrad.2026.112795
Received 12 November 2024; Received in revised form 20 February 2026; Accepted 10 March 2026
Available online 11 March 2026

[9]. This can be challenging in regions such as the brain, where high-resolution, artifact-free images are crucial for accurate diagnosis. Several authors have emphasized that no single technique is ideal for all applications, and the best technique for a particular patient will depend on the specific clinical scenario [10,11].

A recently developed sequence called NeuroMix can generate T1w, T2w, T2 FLAIR, DWI, and 3D-EPI contrasts, including susceptibility-weighted imaging, in one MRI sequence taking between 1:20 and 4 min for a full, unenhanced brain scan [12]. This method includes motion robust single-shot and k-space segmented sequences to perform both EPI and fast spin echo (FSE) readouts, reducing the time for a typical 5-contrast examination by about 80%. While this initial report suggests good performance for diagnosis of several neurological conditions, the method is still limited by relatively low resolution, susceptibility artifacts, and issues with CSF and fat suppression. These factors could limit applicability to detect and classify certain diseases properly, such as edema in amyloid-related imaging abnormalities (ARIA-E), which can be subtle and require excellent fluid suppression technique [13].

A recent comprehensive review of AI-based fast MR imaging covered most of the recently developed models [14]. The authors concluded that although these methods outperform conventional methods, motion artifacts may not be effectively addressed. There remains a need for fast imaging, which can mitigate motion at its root source, and for AI methods to enhance the quality of these images. In this study, we developed and qualitatively evaluated three separate supervised transformer-based models to enhance the image quality of the fast NeuroMix MR protocol. Using conventional images with longer acquisition times as the ground truth, we trained a model to improve the quality of NeuroMix images and assessed them using signal processing methods and a clinical reader study.

2. Material and methods

This retrospective study was approved by the Stanford University Administrative Panel on Human Subjects in Medical Research (Institutional Review Board), eProtocol 26,147 (IRB registration 6208), approved on 22 January 2024, with a waiver of authorization under 45 CFR 164.512(i)(2)(ii)(A, B, C). The authors independently managed the incorporation of any conflicting data or information.

2.1. Patient population

All studies were performed as part of clinical care, where the NeuroMix sequence is obtained immediately after scout imaging to provide images in the case that the patient cannot tolerate the standard protocol. This sequence was added to our institution's routine brain and stroke MRI protocols, and the scans were exclusively performed in patients coming from the emergency department or the inpatient wards with typical clinical indications for MR imaging. This cohort included 350 consecutive studies (mean age: 64 yrs, standard deviation [SD], 17 years; 155 male) and were gathered in 2022. More details about the cohort are provided in Table 1.

Table 1
Demographic and clinical features.

	Mean (y)	SD	
Age	64.7	17.5	
	Female	Male	
Sex	195	155	
Diagnosis	Normal	Abnormal[a]	Minor findings
	101	106	143

Abnormalities included acute infarct, subacute infarct, cranial nerve lesions, cavernous malformation, intraparenchymal hematoma, non-traumatic SAH, amyloid angiopathy, demyelination, aneurysm, and post-XRT susceptibility changes.
SD: Standard Deviation

2.2. MRI data acquisition

All studies were performed at 3 T (Premier or MR750, GE Healthcare, USA). All subjects underwent a fast NeuroMix sequence (2.5 min) and conventional imaging. The T1w, T2w, and FLAIR sequences were selected for evaluation of image quality, as the conventional imaging for these sequences had significantly higher resolution and image quality compared to the NeuroMix images. The summed image duration of the three NeuroMix sequences required 1 min (all sequences take 2.5 min), while the summed image duration of the three conventional sequences was 12.3 min. The imaging acquisition parameters for both the NeuroMix and the conventional imaging are summarized in Table 2.

2.3. Data pre-processing

All the conventional images were resampled to the dimensions of the NeuroMix size to reduce the computational cost. The images were co-registered using Elastix software [15,16], followed by visual examination, with manual re-registration of any failed cases. The images underwent N4 bias field correction with SimpleITK [17]. The images were normalized between 0–1 and the values higher than 95% percentile were capped at 1. Subsequently, the images were cropped to 176 × 224 × 144 size. Finally, all images were registered to a standard brain template defined into the standard MNI stereotactic space using Elastix software.

2.4. SwinUNETR model implementation

This study was conducted and reported in accordance with the CLAIM (Checklist for Artificial Intelligence in Medical Imaging) guidelines, and the completed checklist is provided as supplementary material [18,19].

An attention-based transformer, inspired from [20], was trained to transform the low resolution NeuroMix images to conventional images. The design includes an encoder, a bottleneck, a decoder, and skip connections, primarily built around the Swin-transformer (Shifted windows) module [20]. Images were divided into non-overlapping blocks and linearly projected to create network input sequences. The encoder used patch-merging blocks for signal down-sampling and Swin-transformer blocks for representation learning, forming a hierarchical representation. At the end of the encoder, a bottleneck made up of two sequential Swin-transformer blocks, without any up- or down-sampling, was used to create additional links between the encoder and decoder.

The Swin-transformer block, based on the concept of shifted-windows [20], uses a regular division of patches at one level and a shifted version at the next, enabling connections between varying window shapes via self-attention. The block includes a layer-norm (LN), multihead self-attention (MSA), multi-layer perceptrons (MLP), and several skip-connections. The architecture of the SwinUNETR is illustrated in Fig. 1. Five fold cross validation was performed for training and testing.

The model was implemented in Python using the MONAI framework built on PyTorch. All model training and inference were performed on a workstation equipped with a NVIDIA Tesla V100-SXM2 GPU (32 GB VRAM) and an Intel Xeon E5-2698 v4 CPU. Each model (T1w, T2w, FLAIR) required approximately 17 h for training (5-fold cross-validation) and around 30 s per volume for inference. The NeuroMix-DL framework is therefore computationally efficient and suitable for near real-time deployment in clinical workflows.

The models input are the NeuroMix-derived T1w, T2w, and FLAIR images, where the corresponding conventional T1w, T2w, and FLAIR images serve as the training targets (ground truth). All training data were fully paired, with each NeuroMix T1w, T2w, and FLAIR volume matched to its corresponding conventional volume from the same subject; paired samples were shuffled at the subject level prior to training, and the model was trained using a 3D volume-based approach.

Table 2
Imaging acquisition parameters.

Imaging Parameter	T1		T2		FLAIR	
	Conventional	NeuroMix	Conventional	NeuroMix	Conventional	NeuroMix
Acquisition plane	Axial (GRE)	Axial (EPI)	Axial (SE)	Axial (SSFSE)	Axial (SE)	Axial (SSFSE)
Repetition time (msec)	7.2	17	4991	3850	6000	30,000
Echo time (msec)	2.9	7.4	96	156	114	156
Flip angle (degrees)	9	90	111	90	90	90
Slice thickness (mm)	2	1.2	3	5	2	5
Acquisition matrix	512 × 512	256 × 256	512 × 512	256 × 256	512 × 512	256 × 256
Acquisition time (msec)	101	22	101	15	95	23
Time reduction (%)		78%		85%		76%

GRE: Gradient Echo Sequences, EPI: Echo Planar Imaging, SE: Spin Echo,
SSFSE: Single Shot Fast Spin Echo.

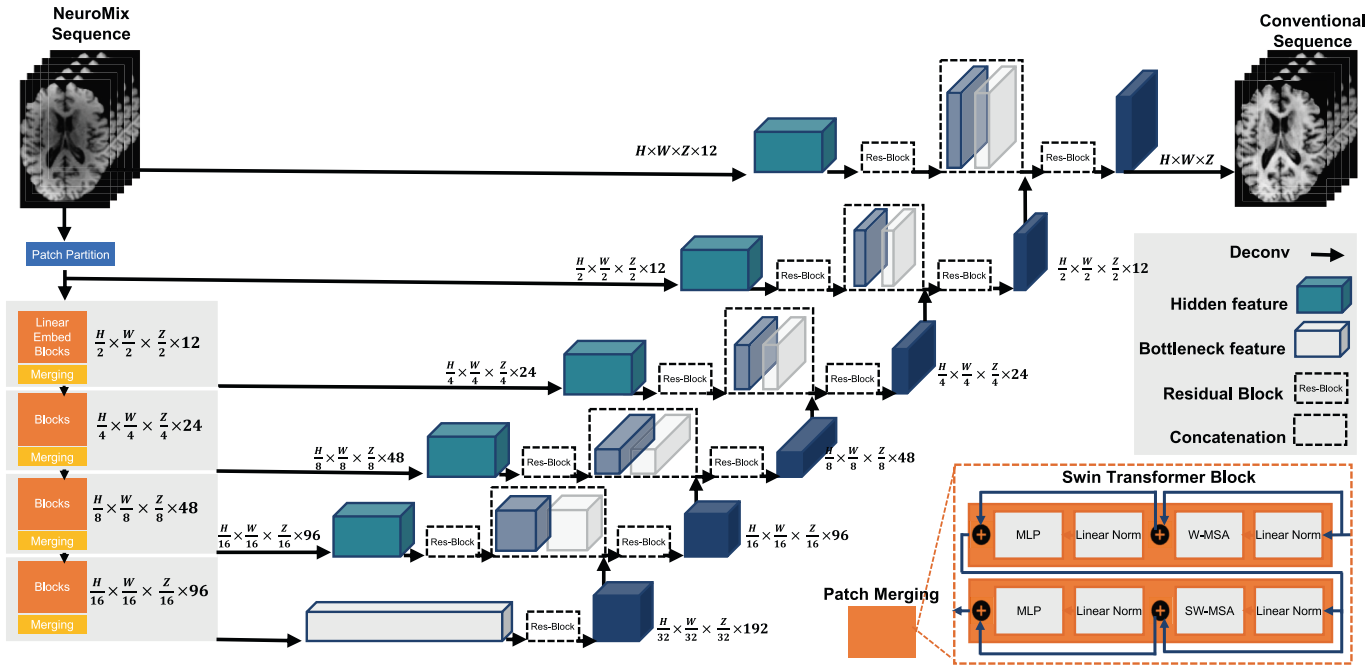

Fig. 1. Overview of the Swin UNETR architecture. The input to the model is a 3D NeuroMix MRI image volume, with different models trained for T1, T2 and FLAIR separately. The SwinUNETR creates non-overlapping patches of the input data and uses a patch partition layer to create windows with a desired size for computing the self-attention. The encoded feature representations in the Swin transformer are fed to a CNN-decoder via skip connections at multiple resolutions. For training, the output of model was the corresponding conventional sequence with higher resolution.

2.5. Assessments of image quality

The predicted images were first visually inspected for any possible artifacts or unexpected abnormalities. Standard signal processing metrics such as the Structural Similarity Index (SSIM) [21] (Eq. (1), Root Mean Squared Error (RMSE) (Eq. (2), and Peak Signal-to-Noise Ratio (PSNR) (Eq. (3), were calculated between the NeuroMix and NeuroMix-DL images by assuming the conventional images as ground truth.

$$\mathrm{SSIM}(x,y) = \frac{(2\mu_x\mu_y + c_1)(2\sigma_{xy} + c_2)}{(\mu_x^2 + \mu_y^2 + c_1)(\sigma_x^2 + \sigma_y^2 + c_2)} \quad (1)$$

Here, μ_x, μ_y represent the average of x (Predicted image), and y (Reference image) images and σ_x^2, σ_y^2 represent their variance, respectively. σ_{xy} denotes the covariance between the x and y images. $c_1 = (k_1 L)^2$, $c_2 = (k_2 L)^2$, k_1=0.01 andk_2 = 0.03 were selected by default to prevent division by very small numbers (L is the dynamic range of the pixel values).

$$\mathrm{RMSE}(x,y) = \sqrt{\frac{1}{N}\sum_{i=1}^{N}(x_i - y_i)^2} \quad (2)$$

Here, N is the total number of voxels in predicted or reference images.

$$\mathrm{PSNR}(x,y) = 20.\log_{10}\left(\frac{x_{max}}{\mathrm{RMSE}(x,y)}\right) \quad (3)$$

In Eq. (3), x_{max} is the maximum value of the predicted image.

Difference maps between the NeuroMix and NeuroMix-DL images and conventional images were generated to highlight the level of error before and after the transformation. To assess whether the method led to improved spatial resolution, we measured the full-width half maximum (FWHM) of the septal nuclei, a structure typically <7.5 mm in most adults [22].

The NeuroMix-DL and the NeuroMix images of each data set were anonymized, their series numbers were randomized and along with the corresponding conventional image presented to a board-certified neuroradiologist with 3 years of experience. For each assessment, the reader evaluated the conventional image and an unknown image (either

NeuroMix or NeuroMix-DL) and assigned an image quality score to the unknown image using a five-point scale: 1, uninterpretable; 2, poor; 3, adequate; 4, good; and 5, excellent. 72 T1w, 72 T2w and 89 FLAIR images were chosen randomly for clinical evaluation. To evaluate intra-reader agreement, 20 subjects were read twice.

2.6. Statistical analysis

A pairwise *t*-test was calculated to evaluate the values of the qualitative and quantitative metrics across the various image processing approaches. The mean reader scores for NeuroMix and NeuroMix-DL and each sequence were calculated and reported separately. The percent change in quality score improvement after applying deep learning method was calculated. The Intraclass Correlation Coefficient (ICC) was used to evaluate intra-reader reproducibility. Significance was considered at the P = 0.05 level, adjusting for multiple comparisons. Statistical analyses were performed using MedCalc® version 22.009 (MedCalc Software Ltd, Ostend, Belgium). ICC values were interpreted as follows: values <0.5 indicate poor reliability, 0.5–0.75 moderate, 0.75–0.90 good, and >0.90 excellent reliability.

3. Results

3.1. Assessment of image quality

Qualitatively, the NeuroMix-DL images showed marked improvement in image quality compared with the NeuroMix images and visually resemble the conventional ground truth images in patients with and without pathological changes (Fig. 2, extra examples in Supplemental Figs. 1-3). The clinical reader observed several cases in which the conventional images were affected by motion artifacts, while the shorter acquisition time of the NeuroMix and NeuroMix-DL sequences appeared to reduce the likelihood of such artifacts (Fig. 3). The NeuroMix-DL images had higher PSNR and SSIM and lower RMSE in all sequences when compared to the original NeuroMix images (Table 3). The model reduced the RMSE by 42 ± 3% (0.12 to 0.07), 33 ± 2% (0.09 to 0.06), and 33 ± 9% (0.12 to 0.08) and improved the SSIM by 5 ± 3% (0.82 to 0.86), 5 ± 1% (0.83 to 0.87) and 4 ± 4% (0.71 to 0.74) for T1, T2, and FLAIR, respectively (p-values all <0.001). There was evidence that the method improved spatial resolution. The FWHM of the septal nuclei for the conventional images was 7 ± 3 mm, while for standard NeuroMix and NeuroMix-DL, the corresponding measurement was 12 ± 3 mm and 9 ± 2 mm (p < 0.001) (Fig. 4).

While the model could enhance the quality of NeuroMix images, it was unable to address artifacts present on the original NeuroMix images (Fig. 5). For example, one subject had NeuroMix-related artifacts from a right parietal ventriculoperitoneal shunt that limited evaluation of the surrounding brain parenchyma in the right parietal and occipital lobes, which were not improved following the application of the deep learning model. We also observed several cases in which the model created a grid artifact for some slices which otherwise remained interpretable. As expected, for subjects with motion artifact during NeuroMix acquisition, the error was propagated to the model's output.

3.2. Clinical readings

The image quality scores, assigned by the reader to each of the NeuroMix and NeuroMix-DL volumes for each sequence, are shown in Fig. 6 along with mean scores and the overall quality enhancement percentage. The mean image quality score for the NeuroMix-DL images was improved by 12 ± 8% (3.1 ± 0.6 to 3.5 ± 0.5), 17 ± 11% (2.8 ± 0.6 to 3.3 ± 0.6), and 15 ± 6% (3.3 ± 0.7 to 3.8 ± 0.7) for T1w, T2w, and FLAIR respectively, compared to the original NeuroMix images. For all the sequences and cases, the number of low scores (1-uninterpretable, 2-poor, and 3-adequate) were reduced significantly after applying our model (p < 0.001)). The intraclass correlation coefficients for the intra-reader agreement study were 0.81 (95% CI: 0.79 to 0.92), 0.87 (95% CI: 0.78 to 0.94) and 0.76 (95% CI: 0.69 to 0.89) for T1w, T2w, and FLAIR images, respectively, which indicate good intra-reader reliability (Table 4).

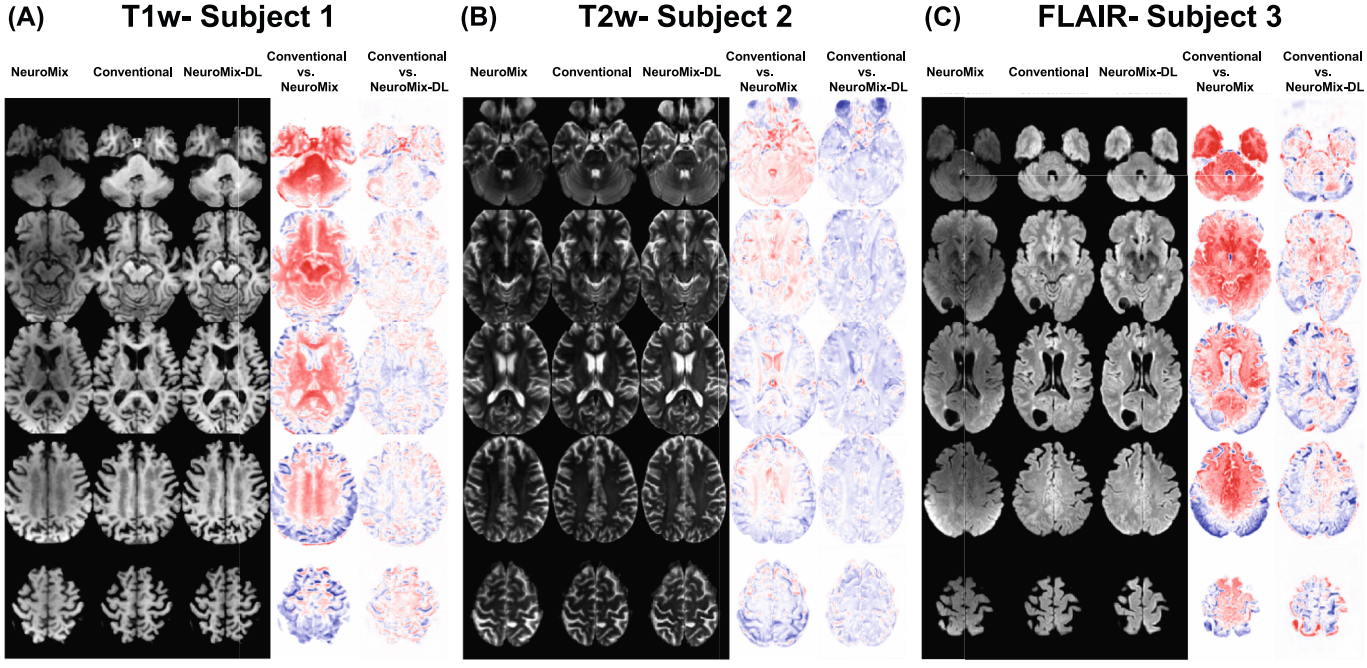

Fig. 2. The performance of the model on T1-weighted, T2-weighted, and FLAIR sequences for different subjects (A- 67 year-old female, B- 38 year-old male, and C-58 year-old female). The first column is the NeuroMix sequence, which is the input to the model, the second column is conventional sequence as ground truth, and the third column is the 'output of model. The fourth and fifth columns show the difference map between the conventional and NeuroMix images and conventional and NeuroMix-DL images. Difference color scale: −0.1 to + 0.1; red = overestimation, blue = underestimation relative to the conventional image.

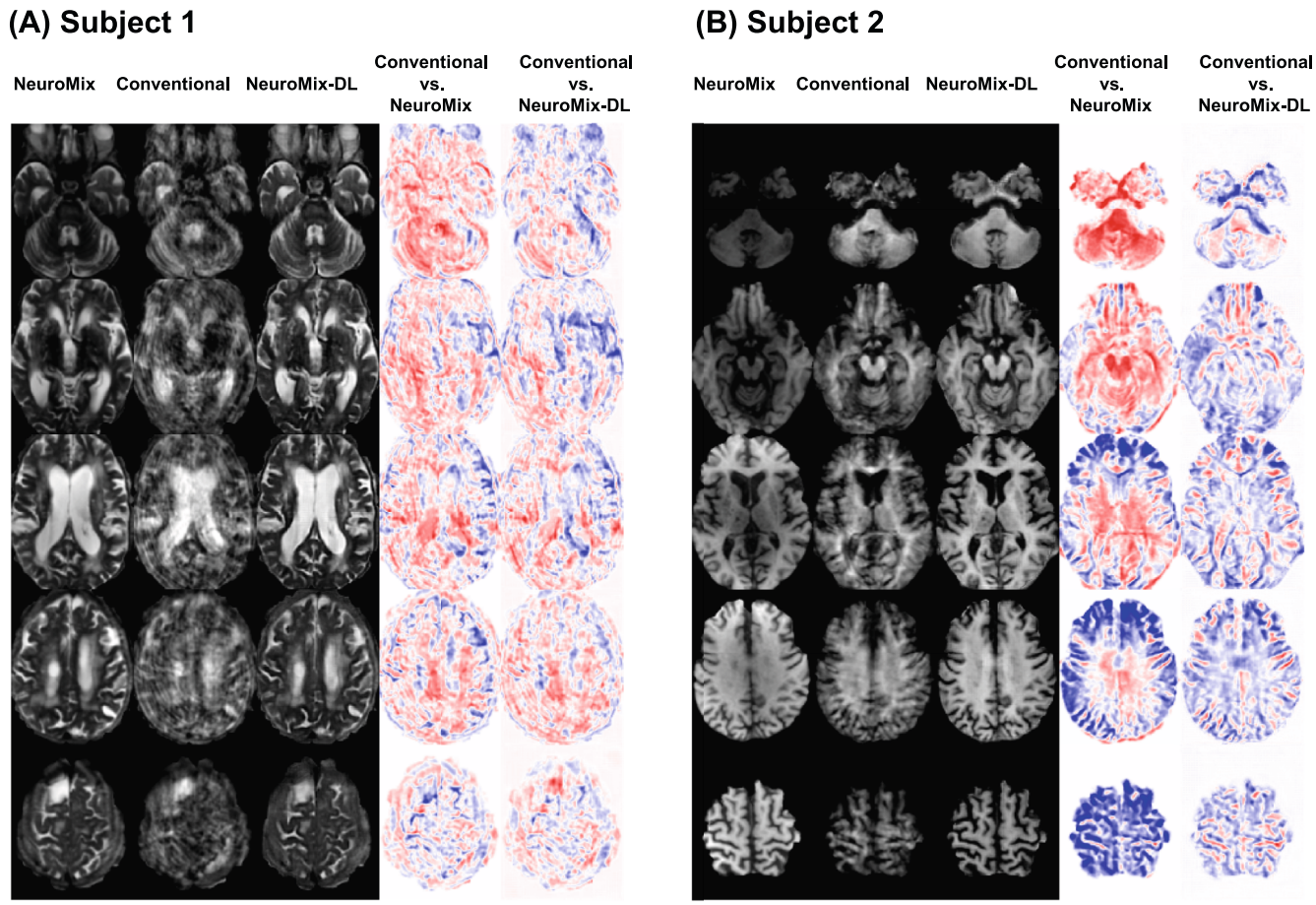

Fig. 3. Examples of motion and susceptibility artifact on conventional MR images that obscures evaluation of adjacent surrounding structures. In these cases (A- 65 year-old female and B- 73 year-old male) the NeuroMix and NeuroMix-DL images are not affected. The fourth and fifth columns show the difference map between the conventional and NeuroMix images and conventional and NeuroMix-DL images. Difference color scale: −0.1 to + 0.1; red = overestimation, blue = underestimation relative to the conventional image.

Table 3
Quantitative signal processing assessment of the NeuroMix and NeuroMix-DL images considering the conventional images as reference. For all three metrics, higher peak signal-to-noise ratio (PSNR), higher structural similarity (SSIM), and lower root mean square error (RMSE), the NeuroMix-DL images are superior. All pair-wise t tests had P values less than 0.001.

	T1w		T2w		FLAIR	
	Average	SD	Average	SD	Average	SD
PSNR Conv v NeuroMix	18.23	0.23	20.91	0.50	18.55	0.28
SSIM Conv v NeuroMix	0.82	0.01	0.83	0.02	0.71	0.01
RMSE Conv v NeuroMix	0.12	0.00	0.09	0.01	0.12	0.00
PSNR Conv v NeuroMix-DL	23.96	0.52	25.16	0.58	21.95	0.70
SSIM Conv v NeuroMix-DL	0.86	0.03	0.87	0.02	0.74	0.03
RMSE Conv v NeuroMix-DL	0.07	0.00	0.06	0.00	0.08	0.01
% PSNR increase	31.4	2.2	20.4	1.0	18.3	5.2
% SSIM increase	4.8	2.9	4.8	1.1	4.2	3.5
% RMSE decrease	41.7	3.0	33.3	2.1	33.3	8.8

SD: Standard Deviation, SSIM: Structural Similarity Index Metric, PSNR: Peak Signal-to-Noise Ratio, RMSE: Root Mean Square Error.

4. Discussion

This study aimed to assess the performance of a transformer-based model for enhancing the image quality for NeuroMix, a fast multi-contrast acquisition sequence. The transformer based models are an active research field initiated by [20], aiming to apply the self-attention capabilities of transformers, successful in natural language processing, to image and vision related tasks. The NeuroMix protocol enables the acquisition of five separate MR contrasts in about 2–3 min, including full brain coverage. The T1w, T2w, and FLAIR low-quality images acquired by NeuroMix were used separately as input of three transformer-based models and the corresponding high-quality images (acquired by conventional clinical protocol) were used as the target for synthesis. In contrast to previous studies [23,24], which used different compressed sensing methods such as undersampled k-space to generate the low-quality images as input, we reconstructed the MR images directly from a well-established protocol which does not have the limitations of other fast scanning methods. The NeuroMix sequence contains motion-robust single-shot sequences using EPI and FSE readouts (without EPI distortions). This method is less affected by leakage artifacts that can occur in

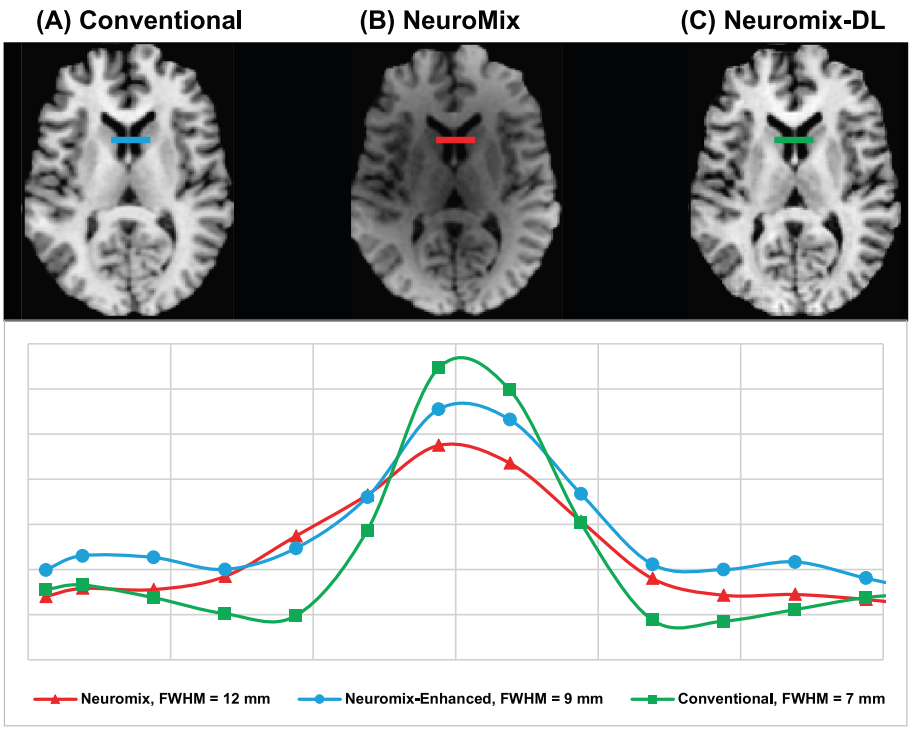

Fig. 4. Septal nuclei intensity line profiles measurements for a 61-year-old female. Axial views from T1-weighted images of conventional (A), NeuroMix (B), and NeuroMix-DL (C) images. The septal nuclei signal intensity line profiles are shown below. NeuroMix-DL images demonstrate increased spatial resolution as measured by the decreased width of this fine structure compared with the acquired NeuroMix images.

simultaneous multi-slice imaging or streaking artifacts that can affect radial imaging.

We have shown that the NeuroMix-DL images had a smaller RMSE compared with the NeuroMix images and a greater mean image quality score as assessed with multiple image quality metrics and visual judgment of an academic neuroradiologist. The reconstructed images were observed to have sharper edges and reduced noise based on qualitative assessment by the neuroradiologist, and this was quantitatively supported by increased PSNR values compared to the original NeuroMix images. While transformer-based methods have been used to enhance image quality for different MRI applications [25,26], it is critical to validate whether they generalize beyond a particular scanner or practice setting, given that many deep learning algorithms have shown worse performance when applied to external test sets [27]. Moreover, these cases were gathered sequentially, limiting selection bias and reflecting the potential application of the algorithm in a real-world clinical setting.

Several studies have sought to improve images acquired with undersampled k-space using transformers. In a recent study, a Swin Transformer model was compared with other CNN models in the task of compressed sensing, showing superior performance [28]. Other studies such as Lorenzana et al. showcased the advantages offered by Kaleidoscope token embeddings [29]. These embeddings offer enhanced global image representations for low-frequency signals. They concluded that the improvement was attributed to superior ability of transformers to model global features, particularly compressed sensing artifacts. In another study, the authors suggested a transformer-based model for MR image super resolution reconstruction which consists of a multi-level feature extraction module and a reconstruction module [30]. Their model links frequency domain and spatial domain loss functions to preserve the image details during image reconstruction. They showed their model can generate high-resolution images with SSIM of 0.91 and mean absolute error of 25.82 from images with the sampling ratio of 50%, but did not perform a reader study to understand the clinical performance of their model. ReconFormer is a model which uses recurrent transformer models to progressively rebuild high-quality MR images using highly under-sampled k-space data, achieving up to an 8-fold acceleration [31]. MFormer is an expedited MRI reconstruction transformer comprised of cascading MFormer blocks housing multi-scale Dynamic Deformable Swin Transformer (DST) modules. The DST modules align adjacent slice features implicitly, utilizing dynamic deformable convolution, and extract both local and non-local features before merging information [32]. In this study we used the advantages of transformers as shown by these previous studies, to improve the quality of a cutting-edge fast MR imaging sequence that can produce multiple contrasts and evaluated the performance of the model both clinically and quantitatively.

Although direct comparison across studies is limited due to differences in image size, preprocessing pipelines, and acceleration settings, we contextualized our results by comparing relative improvements reported in related work. For example, Huang et al. reported that, under a 30% sampling mask (about 70% k-space reduction), SwinMR increased PSNR by about 32% for FLAIR (from 28.74 to 37.97) and by about 43% for T1 (from 28.82 to 41.08), with SSIM increasing by about 58% to 61% (from about 0.60 to about 0.94 to 0.95) compared with zero-filled baseline [33]. Dar et al. reported that, at 6x acceleration (about 83% k-space reduction), PSFNet improved PSNR by about 6% for cT1 (from 35.8 to 37.8) and SSIM by about 3% (from 0.916 to 0.944) compared with a conventional parallel imaging baseline (SPIRiT), with similar trends for T2 [34]. In our study, NeuroMix-DL improved PSNR relative to NeuroMix by 31.4% (from 18.23 to 23.96) for T1w, 20.4% (from 20.91 to 25.16) for T2w, and 18.3% (from 18.55 to 21.95) for FLAIR, with SSIM improvements of 4.9% (from 0.82 to 0.86), 4.8% (from 0.83 to 0.87), and 4.2% (from 0.71 to 0.74), while leveraging the previously reported NeuroMix acquisition time reduction of about 80% versus conventional multi contrast imaging.

Direct comparison across studies should still be interpreted cautiously because most accelerated MRI reconstruction papers create undersampled inputs retrospectively from the same fully sampled k-space, so the input and ground truth images are perfectly aligned voxelwise, which favours higher PSNR and SSIM. In contrast, our ground

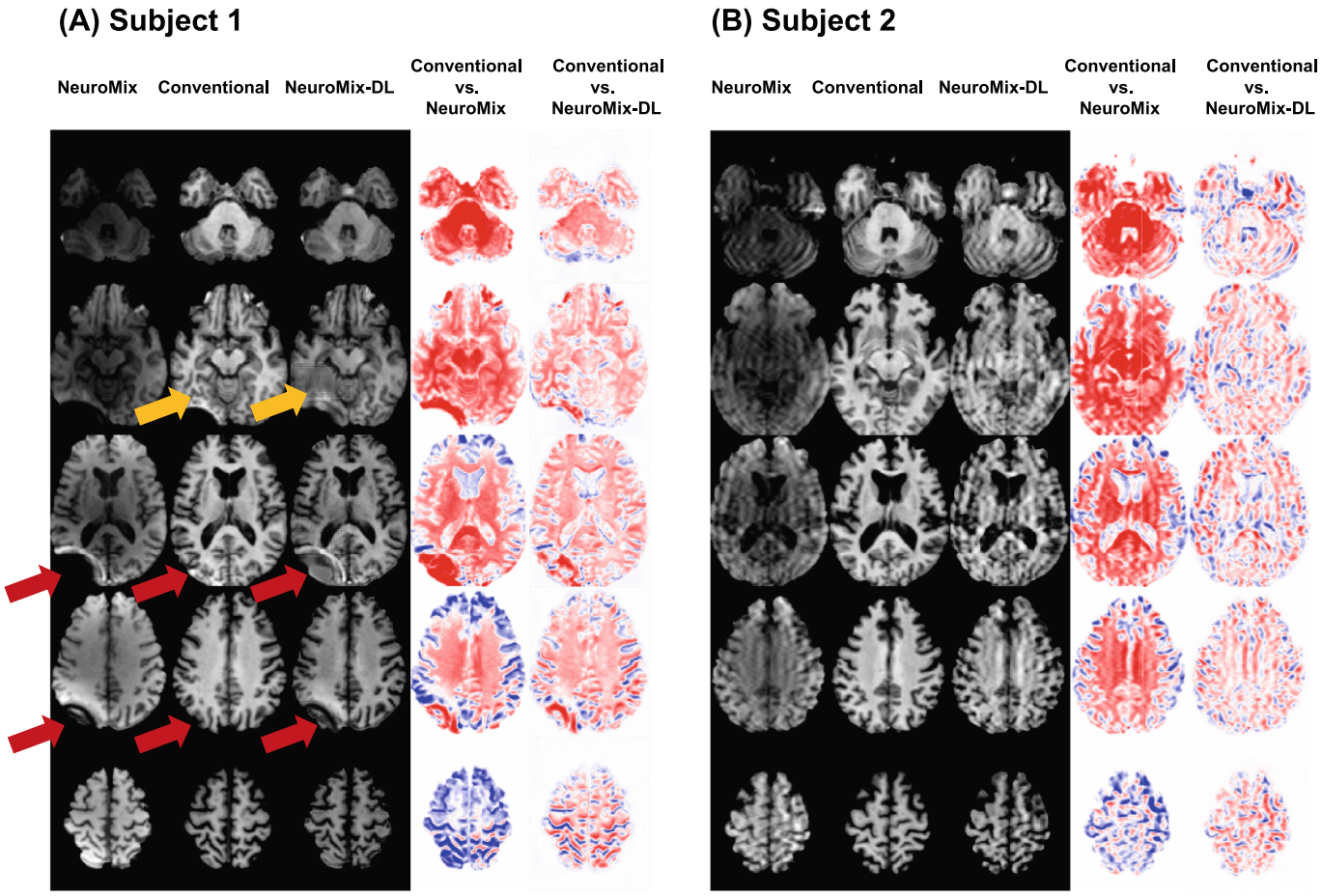

Fig. 5. Artifacts seen in two subjects (A- 58-year-old female and B- 49-year-old male). The panel A shows a subject with artifacts on NeuroMix T1-weighted imaging from a right parietal ventriculoperitoneal shunt, which limits detailed evaluation of the surrounding brain parenchyma in the right parietal and occipital lobes (red arrow). For a few cases, the model causes a grid artifact for some slices (orange arrow). The panel B shows a subject with motion artifact during NeuroMix acquisition, which propagated to the model's output. The fourth and fifth columns show the difference map between the conventional and NeuroMix images and conventional and NeuroMix-DL images. Difference color scale: −0.1 to + 0.1; red = overestimation, blue = underestimation relative to the conventional image.

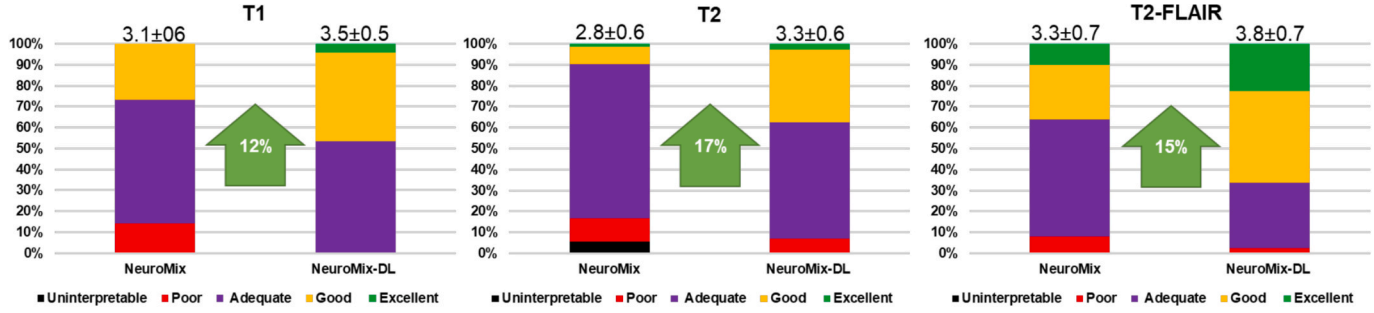

Fig. 6. Clinical image quality scores (1 = uninterpretable, 5 = excellent; mean scores and standard deviation of all readings presented at top of each bar) for T1, T2 and FLAIR sequences assigned by the one reader. The green arrows show the mean percent improvement for the NeuroMix-DL images (all $p < 0.001$).

Table 4
The Intraclass Correlation Coefficient (ICC) for intra-reader reliability. ICC values less than 0.5 indicate poor reliability, between 0.5 and 0.75 moderate reliability, between 0.75 and 0.9 good reliability, and greater than 0.90 excellent reliability.

	T1		T2		FLAIR	
	ICC	95% CI	ICC	95% CI	ICC	95% CI
Single measures	0.81	0.79 to 0.92	0.87	0.78 to 0.94	0.76	0.69 to 0.89

truth is an independently acquired conventional sequence and NeuroMix is a real fast acquisition. Hence, co-registration and residual distortion or motion differences between acquisitions can reduce PSNR and SSIM, even when the clinical appearance and reader rated quality improve.

The NeuroMix-DL images received notably higher ratings. This could be attributed to two factors. First, the algorithm's extensive training on a diverse range of cases results in additional noise reduction alongside the intended super-resolution capabilities. Second, the reduced acquisition times may limit the occurrence of motion-induced artifacts in patients.

Quicker scans can also have a significant impact on patient satisfaction and their ability to endure an MRI procedure, as up to 30% of patients experience anxiety during examinations, largely due to claustrophobia [1]. It should be noted that artifacts related to fast scanning were not entirely removed using this approach, particularly susceptibility artifact.

The present study is subject to several limitations. First, the sample size was relatively small, there were limitations in the types of pathologies included, and all images came from a single center (though with different individual scanner models). Future studies should consider evaluating larger patient cohorts across multiple sites. This is especially important for small lesions, as there are concerns about potential loss of information in deep learning reconstruction [35]. However, a recent empirical study found that transformer-based reconstruction methods are robust to minimal changes and can accurately capture fine details [23]. Also, there has not yet been a study to evaluate the clinical performance of either NeuroMix or the use of NeuroMix-DL images with respect to their utility in clinical practice, partially because of the recent introduction of the method. Finally, the reader study did not include all the images that were assessed with signal processing metrics, due to the limited time and availability of the clinical reader. Evaluating AI algorithms using reader studies is essential to understand performance in clinical practice, but challenging to implement due to the high cost of performing such studies.

While our proposed method shows promising results, it is important to consider its application within the clinical context. The method should currently serve as an adjunct to, rather than a replacement for, conventional clinical decision-making processes. Further studies, including prospective clinical trials, are required to validate its performance and reliability in real-world settings.

In conclusion, our findings indicate that high-resolution imaging studies could be significantly shortened by applying AI techniques to NeuroMix multi-contrast MRI, improving the patient experience, scanner efficiency, and reducing costs without compromising diagnostic quality. However, further research is needed to evaluate the clinical performance and reliability of NeuroMix-DL images in clinical settings.

Funding information

Swiss National Science Foundation under grant SNSF 320030_176052, and American Heart Association Grant #826254.

CRediT authorship contribution statement

Amirhossein Sanaat: Writing – review & editing, Writing – original draft, Visualization, Validation, Software, Resources, Project administration, Methodology, Investigation, Formal analysis, Data curation, Conceptualization. **Johannes Hugo Decker:** . **Ramy Hussein:** Writing – review & editing, Supervision. **Moss Y Zhao:** Writing – review & editing, Writing – original draft, Conceptualization. **Habib Zaidi:** Writing – review & editing, Writing – original draft, Supervision, Funding acquisition. **Tim Sprenger:** Writing – review & editing. **Stefan Skare:** Writing – review & editing, Writing – original draft. **Michael Moseley:** Writing – review & editing, Writing – original draft, Supervision. **Greg Zaharchuk:** Writing – review & editing, Writing – original draft, Supervision, Resources, Project administration, Investigation, Funding acquisition, Formal analysis, Data curation, Conceptualization.

Declaration of competing interest

The authors declare the following financial interests/personal relationships which may be considered as potential competing interests: This research study obtained a waiver of consent from our Institutional Review Board due to its retrospective, observational design. Two of the authors report potential conflicts of interest. Tim Sprenger is an employee of GE Healthcare and Greg Zaharchuk has equity interest in Subtle Medical and is a consultant for Bracco and Bayer Healthcare. No products from these companies were used in this study.

Acknowledgements

This work was supported by Swiss National Science Foundation under grant SNSF 320030_176052 and an American Heart Association Grant #826254.

Appendix A. Supplementary data

Supplementary data to this article can be found online at https://doi.org/10.1016/j.ejrad.2026.112795.

Data availability

Data analyzed during the study were provided by a third party. Requests for data should be directed to the provider indicated in the Acknowledgements.

References

[1] J.C. Meléndez, E. McCrank, Anxiety-related reactions associated with magnetic resonance imaging examinations, JAMA 270 (6) (1993) 745–747.
[2] R. Turner, D. Le Bihan, J. Maier, et al., Echo-planar imaging of intravoxel incoherent motion, Radiology 177 (2) (1990) 407–414.
[3] S. Skare, T. Sprenger, O. Norbeck, et al., A 1-minute full brain MR exam using a multicontrast EPI sequence, Magn. Reson. Med. 79 (6) (2018) 3045–3054.
[4] K.G. Hollingsworth, Reducing acquisition time in clinical MRI by data undersampling and compressed sensing reconstruction, Phys. Med. Biol. 60 (21) (2015) R297–R322.
[5] D.K. Sodickson, W.J. Manning, Simultaneous acquisition of spatial harmonics (SMASH): fast imaging with radiofrequency coil arrays, Magn. Reson. Med. 38 (4) (1997) 591–603.
[6] G.H. Glover, J.M. Pauly, Projection reconstruction techniques for reduction of motion effects in MRI, Magn. Reson. Med. 28 (2) (1992) 275–289.
[7] J.G. Pipe, Motion correction with PROPELLER MRI: application to head motion and free-breathing cardiac imaging, Magn. Reson. Med. 42 (5) (1999) 963–969.
[8] D.C. Peters, F.R. Korosec, T.M. Grist, et al., Undersampled projection reconstruction applied to MR angiography, Magn. Reson. Med. 43 (1) (2000) 91–101.
[9] D. Holland, J.M. Kuperman, A.M. Dale, Efficient correction of inhomogeneous static magnetic field-induced distortion in Echo Planar Imaging, Neuroimage 50 (1) (2010) 175–183.
[10] Q. Chen, K.W. Stock, P.V. Prasad, H. Hatabu, Fast magnetic resonance imaging techniques, Eur. J. Radiol. 29 (2) (1999) 90–100.
[11] M. Lang, O. Rapalino, S. Huang, et al., Emerging techniques and future directions: fast and portable magnetic resonance imaging, Magn. Reson. Imaging Clin. N. Am. 30 (3) (2022) 565–582.
[12] T. Sprenger, A. Kits, O. Norbeck, et al., NeuroMix-A single-scan brain exam, Magn. Reson. Med. 87 (5) (2022) 2178–2193.
[13] M. Roytman, F. Mashriqi, K. Al-Tawil, et al., Amyloid-related imaging abnormalities: an update, AJR Am. J. Roentgenol. 220 (4) (2023) 562–574.
[14] Y. Chen, C.B. Schönlieb, P. Liò, et al., AI-based reconstruction for fast MRI—a systematic review and meta-analysis, Proc. IEEE 110 (2) (2022) 224–245.
[15] S. Klein, M. Staring, K. Murphy, et al., Elastix: a toolbox for intensity-based medical image registration, IEEE Trans. Med. Imaging 29 (1) (2009) 196–205.
[16] N. Tzourio-Mazoyer, B. Landeau, D. Papathanassiou, et al., Automated anatomical labeling of activations in SPM using a macroscopic anatomical parcellation of the MNI MRI single-subject brain, Neuroimage 15 (1) (2002) 273–289.
[17] B. Lowekamp, D. Chen, L. Ibanez, D. Blezek, The design of SimpleITK, Front. Neuroinf. 7 (2013).
[18] M.E. Klontzas, Reporting checklists as compulsory supplements to artificial intelligence manuscript submissions, Diagn. Interv. Radiol. 31 (1) (2025) 17–18.
[19] J. Mongan, L. Moy, C.E. Kahn Jr., Checklist for artificial intelligence in medical imaging (CLAIM): a guide for authors and reviewers, Radiol. Artif. Intell. 2 (2) (2020) e200029.
[20] Z. Liu, Y. Lin, Y. Cao, et al., Swin transformer: Hierarchical vision transformer using shifted windows, in: Proceedings of the IEEE/CVF International Conference on Computer Vision, 2021, pp. 10012–10022.
[21] Z. Wang, A.C. Bovik, H.R. Sheikh, E.P. Simoncelli, Image quality assessment: from error visibility to structural similarity, IEEE Trans. Image Process. 13 (4) (2004) 600–612.
[22] M. Sarwar, The septum pellucidum: normal and abnormal, AJNR Am. J. Neuroradiol. 10 (5) (1989) 989–1005.
[23] Darestani MZ, Chaudhari AS, Heckel R. Measuring robustness in deep learning based compressive sensing. International Conference on Machine Learning, 2021. PMLR: 2433-44.

[24] J.D. Rudie, T. Gleason, M.J. Barkovich, et al., Clinical assessment of deep learning-based super-resolution for 3D volumetric brain MRI, Radiol. Artif. Intell. 4 (2) (2022) e210059.
[25] K. Bahrami, F. Shi, X. Zong, et al., Reconstruction of 7T-like images from 3T MRI, IEEE Trans. Med. Imaging 35 (9) (2016) 2085–2097.
[26] W.J. Do, S. Seo, Y. Han, et al., Reconstruction of multicontrast MR images through deep learning, Med. Phys. 47 (3) (2020) 983–997.
[27] J.R. Zech, M.A. Badgeley, M. Liu, et al., Variable generalization performance of a deep learning model to detect pneumonia in chest radiographs: a cross-sectional study, PLoS Med. 15 (11) (2018) e1002683.
[28] Z. Wu, W. Liao, C. Yan, et al., Deep learning based MRI reconstruction with transformer, Comput. Methods Programs Biomed. 233 (2023) 107452.
[29] Lorenzana MB, Engstrom C, Chandra SS. Transformer Compressed Sensing Via Global Image Tokens. 2022 IEEE International Conference on Image Processing (ICIP), 16-19 Oct. 2022 2022. 3011-5.
[30] Yan C, Shi G, Wu Z. SMIR: A Transformer-Based Model for MRI super-resolution reconstruction. 2021 IEEE International Conference on Medical Imaging Physics and Engineering (ICMIPE), 12-14 Nov. 2021 2021. 1-6.
[31] P. Guo, Y. Mei, J. Zhou, et al., ReconFormer: accelerated MRI reconstruction using recurrent transformer, IEEE Trans. Med. Imaging (2023) 1.
[32] Alghallabi W, Dudhane A, Zamir W, et al. Accelerated MRI Reconstruction via Dynamic Deformable Alignment Based Transformer. In: Cao X, Xu X, Rekik I, et al., eds. Machine Learning in Medical Imaging, 2024// 2024. Cham. Springer Nature Switzerland: 104-14.
[33] J. Huang, Y. Fang, Y. Wu, et al., Swin transformer for fast MRI, Neurocomputing 493 (2022) 281–304.
[34] S.U.H. Dar, Ş. Öztürk, M. Özbey, et al., Parallel-stream fusion of scan-specific and scan-general priors for learning deep MRI reconstruction in low-data regimes, Comput. Biol. Med. 167 (2023) 107610.
[35] V. Antun, F. Renna, C. Poon, et al., On instabilities of deep learning in image reconstruction and the potential costs of AI, Proc. Natl. Acad. Sci. U. S. A. 117 (48) (2020) 30088–30095.